Analyzing the effect of residual stresses on the fatigue life of cold-drawn steel wire specimens

Danielle Lopes Zaidan, Paulo Pedro Kenedi, Luís Felipe Guimarães de Souza
Postgraduate Program in Mechanical Engineering and Materials Technology - PPEMM, CEFET-RJ, Brazil
danielle.zaidan@aluno.cefet-rj.br, http://orcid.org/0009-0008-7141-8275
paulo.kenedi@cefet-rj.br, https://orcid.org/0000-0001-5563-843X
luis.souza@cefet-rj.br, https://orcid.org/0000-0002-6669-8451

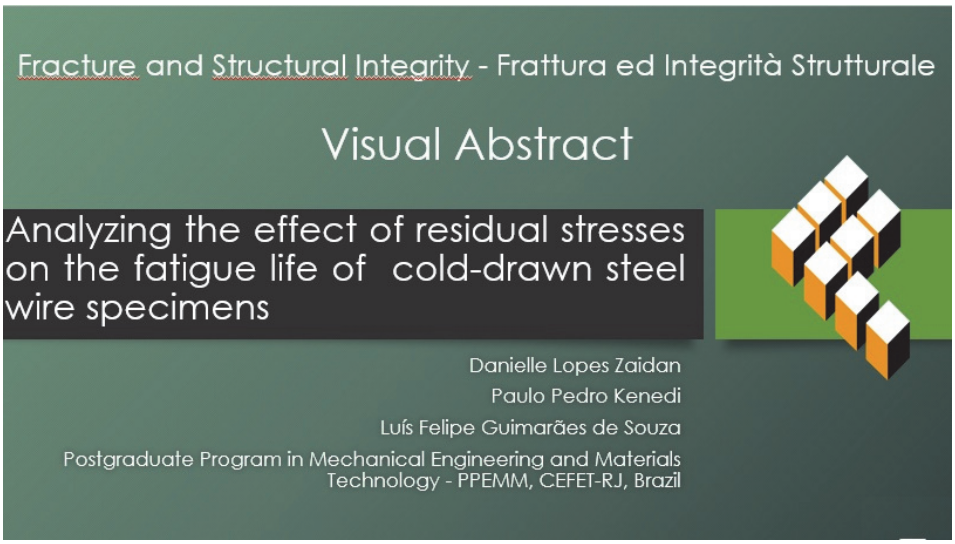

Citation: Zaidan, D. L., Kenedi, P. P., de Souza, L. F. G., Analyzing the effect of residual stresses on the fatigue life of cold-drawn steel wire specimens, Fracture and Structural Integrity, 74 (2025) 42-54.

Received: 27.02.2025
Accepted: 27.06.2025
Published: 09.07.2025
Issue: 10.2025

KEYWORDS. Residual stress, Fatigue, Analytical model.

INTRODUCTION

Fatigue and residual stress are responsible for many mechanical failures. Although there are many areas where fatigue can be applied, such as civil engineering, Laterza et al. [1] or bioengineering, Teoh [2], the focus of this manuscript will be set on mechanical engineering. Most of the residual stress literature references are experimental, as in Tabatabaeian et al. [3]. In this manuscript, however, the residual stress approach will be developed in an analytical way. These two important failure causes, one widely known as fatigue and the other lesser known as residual stress, will be combined to form a compound analytical model. A step-by-step explanation will be given for the residual stress analytic approach, leaving the fatigue basics available in the Appendix. Residual stress can develop in numerous ways in manufacturing processes, such as welding or machining. Any procedure that partially yields a mechanical part cross-section can generate residual stress. Textbooks about the mechanics of solids, such as Crandall et al. [4], present, as a basic subject, the residual stress distribution in static beams submitted to one semi-cycle bending moment, for an elastic perfectly plastic material. Although analytical approaches can be used to gain insight into cross-sectional residual stress distribution, they usually handle only simple geometries, such as rectangular or circular cross-sections. Stok and Halilovic [5] show an elastoplastic analytical solution for bending beams with rectangular cross-sections. Rimovskis and Sabaliauskas[6] analyzed, for rectangular and circular beam cross-sections, the drift of the neutral axis relative to the centroidal axis of the beam as a

function of dissimilar yielding parameters in tension and compression. Castro and Meggiolaro [7] and Jirasek and Bazant[8] presented improvements in residual stress analytical models. De Castro et al. [9] show different cases of analytical models' applications to estimate the residual stress distribution of partially yielded structures of rectangular cross sections. Experimental techniques were used to estimate residual stress on surfaces, as in Schajer [10]. Atienza and Elices [11] analyze the residual stress in cold-drawn wires experimentally and numerically, through the influence of residual stresses on the tensile test, where the residual stress was relieved based on mechanical and/or thermomechanical treatments. Yet, the availability of the combination of fatigue and residual stress, in technical literature, is quite uncommon. One exception is the interesting manuscript of McClung [12], that provides a broad literature survey of the current understanding of significant residual stress issues for fatigue lifetime for shot peening, cold expansion of holes, welding, and machining. Also, see Webster et al. [13], James et al. [14] and Vaara et al. [15] for additional references.
This article proposes an analytical model to describe the effect of residual stress on the fatigue life of partially yielded cold-drawn steel wires, modeled as a bi-linear material, of bulged rectangular cross-section. This research is a development of former references, such as Zaidan et al. [16]. The results obtained in this manuscript can contribute to improving the knowledge about the effect of residual stress on fatigue performance of partially yielded cold-drawn steel wires, extensively used, for instance, in the offshore industry.

ANALYTICAL MODEL

The compound analytical model, which intends to reproduce the experimental part of the manuscript, is divided into residual stress and fatigue approaches, which refer, respectively, to the experimental part of phases 1 and 2. In phase 1, a monotonic displacement is imposed on the specimen, as shown in Fig.1.b. A circular forming tool acts transversally on the specimen, supported by a 3-point bending gripper, yielding partially its cross-section. After spring-back, as shown in Fig.1.c, a residual stress distribution pattern is generated in its cross-section. Phase 1 is described by the residual stress approach of this analytical model, which is considered a relevant contribution, represented by Eqns. (1-11). In phase 2 a variable transverse load P(t) is applied on the specimen that has already passed by phase 1, turned upside down, as shown in Fig. 1.d. The variable transverse load is applied until the specimen completely fails. The phase 2 is described by the fatigue approach of this analytical model. The applied fatigue theory is the classical one, so it was placed in the Appendix section, as shown in Eqns. (1A-7A). The compound analytical model, as shown in Eqns. (12-22), merges two different phenomena, residual stress and fatigue, to produce a comprehensive analysis of the effect of residual stresses on the fatigue life of cold-drawn steel wire specimens. Mathcad software is used to perform calculations.

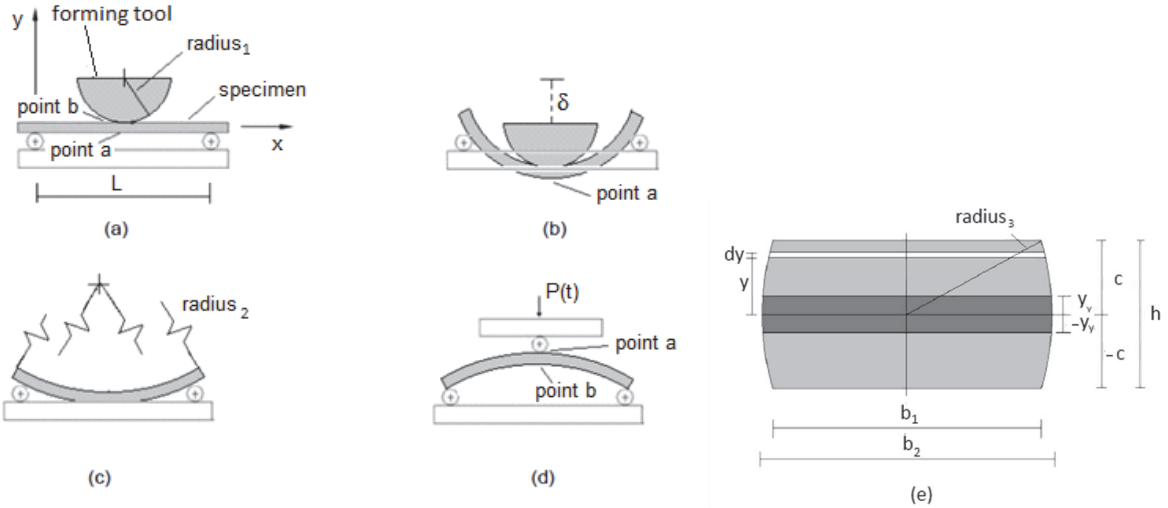

Figure 1: (a) The forming tool, with radius$_1$, touches the specimen, (b) a transversal displacement δ is applied towards the specimen, (c) the specimen, after spring back, presents radius$_2$, (d) the specimen is turned upside down and the fatigue loading is applied, (e) the specimen bulged rectangle cross-section.

Where radius$_1$ is the forming tool radius. Radius$_2$ is the radius of curvature of the specimen after spring back. Radius$_3$ is the radius of the specimen's lateral cross-section. *L* is the length of the specimen between the 3-point bending gripper external rollers. δ is transversal displacement applied towards the specimen. P(t) is the fatigue loading. b_1 and b_2 are, respectively, the

minor and the major width of the specimen's cross-section, *y* is a vertical distance and *dy* is a differential of vertical distance. And *c* is the semi-height and *h* is the height of the specimen's cross-section. y_y is the elastic-plastic border.

Residual stress basics

Every step of the residual stress part of the analytical model is explicitly presented and commented on. The value of the bending moment M(ϱi) imposed by the forming tool is inside the range $M_y < M(\varrho i) < M_p$. The maximum elastic moment M_y and the plastic moment M_p equations are presented.

$$M_y = 2\cdot\left\{\int_0^c y\cdot\frac{y}{c}\cdot S_{y0}\cdot 2\cdot\sqrt{radius_3^2 - y^2}\,dy\right\} \qquad radius_3 = \sqrt{c^2 + \left(\frac{b_1}{2}\right)^2} \tag{01}$$

$$M_p = 2\cdot\left\{\int_0^c y\cdot\left(S_{y0} + E_t\cdot\left(\frac{y}{\rho_i} - \varepsilon_y\right)\right)\cdot 2\cdot\sqrt{radius_3^2 - y^2}\,dy\right\} \tag{02}$$

$$\rho_i = radius_1 + c \qquad radius_2 = \frac{c}{|\varepsilon_a|} \qquad \rho_y = \frac{c}{\varepsilon_y} \qquad \rho_p = \frac{c}{\varepsilon_u} \qquad E_t = \frac{S_{ut0} - S_{y0}}{\varepsilon_u - \varepsilon_y} \tag{03}$$

Where S_{y0} is the material yielding resistance and S_{ut0} is the material's ultimate resistance, both, as received, E_t is the plastic tangent modulus, ρ_i, ρ_y, and ρ_p are the radius of curvature of the specimen, respectively, at loading, at the beginning of yielding, and the full cross-section yielding. The ε_a is the strain at point *a* of Fig 1.a, ε_y is the yielding strain, and ε_u is the ultimate strain. The elastic-plastic border y_y equation is presented:

$$y_y = \varepsilon_y\cdot\rho_i \qquad \rho_p < \rho_i < \rho_y \tag{04}$$

The equation of the bending moment $M(\rho_i)$ in function of the imposed radius of curvature of the specimen:

$$M(\rho_i) = 2\cdot\left\{\int_0^{y_y} y\cdot\left(\frac{y}{\varepsilon_y\cdot\rho_i}\cdot S_{y0}\right)\cdot 2\cdot\sqrt{radius_3^2 - y^2}\,dy + \int_{y_y}^c y\cdot\left(S_{y0} + E_t\cdot\left(\frac{y}{\rho_i} - \varepsilon_y\right)\right)\cdot 2\cdot\sqrt{radius_3^2 - y^2}\,dy\right\}$$

$$M_y < M(\rho_i) < M_p \tag{05}$$

The stress σ and strain ε evolution of the specimen point *a* (shown in Fig. 1.a) is presented in Fig. 2.a, whose values are shown in Eqn. (06), Castro and Meggiolaro [6].

$$\sigma_0 = 0 \qquad \varepsilon_0 = 0$$

$$\sigma_1 = S_{y0} \qquad \varepsilon_1 = \varepsilon_y$$

$$\sigma_2 = S_{y0} + E_t\cdot\left(\frac{y}{\rho_i} - \varepsilon_y\right) \qquad \varepsilon_2 = \left(\frac{y_y}{c}\right)^{-1}\cdot\varepsilon_y$$

$$\sigma_3 = S_{y0} + E_t\cdot\left(\frac{y}{\rho_i} - \varepsilon_y\right) + \sigma_{sb}(-c) \qquad \varepsilon_3 = \left[\left(\frac{y_y}{c}\right)^{-1} - \alpha\right]\cdot\varepsilon_y \tag{06}$$

where, $\alpha = M(\rho_i)/M_y$ is a multiplicative factor. $\sigma_{sb}(-c)$ is the springback stress at specimen point *a*, of Fig 1.a, estimated by Eqn. (10). The Eqns. (07) and (08) represent, respectively, in Fig. 2.a, the material behavior (light gray dash lines) and the loading/unloading equations (black lines for point *a*, and gray lines for point *b*), where points *a* and *b* are shown in Fig 1.a.

$$\sigma_s(\varepsilon) = \begin{cases} -S_{y0} + E_t \cdot (\varepsilon + \varepsilon_y), & \varepsilon < -\varepsilon_y \\ \dfrac{S_{y0}}{\varepsilon_y} \cdot \varepsilon, & -\varepsilon_y \le \varepsilon \le \varepsilon_y \\ S_{y0} + E_t \cdot (\varepsilon - \varepsilon_y), & \varepsilon > \varepsilon_y \end{cases} \tag{07}$$

$$\sigma(\varepsilon) = \begin{cases} \dfrac{S_{y0}}{\varepsilon_y} \cdot \varepsilon & \varepsilon_0 \le \varepsilon \le \varepsilon_1 \\ S_{y0} + E_t \cdot (\varepsilon - \varepsilon_y) & \varepsilon_1 \le \varepsilon \le \varepsilon_2 \\ \dfrac{\sigma_3 - \sigma_2}{\varepsilon_3 - \varepsilon_2} \cdot \varepsilon + \dfrac{\sigma_2 \cdot \varepsilon_3 - \sigma_3 \cdot \varepsilon_2}{\varepsilon_3 - \varepsilon_2} & \varepsilon_2 \le \varepsilon \le \varepsilon_3 \end{cases} \tag{08}$$

In Fig. 2.a, in the final state of point *a*, labeled with the number 3, there is a change in the stress signal from its former state, labeled with the number 2, while the strain signal remains the same signal. Also, in Fig. 2.a the abscissa axis was maintained as strain (not divided by ε_{y0}) to show that at the end of phase 1, point *a* has a residual strain of 0.06 (or 6%). The Eqns. (09-11) were used to build the various cross-section stress distributions in Fig. 2.b.

$$\sigma_{curv}(y) = \begin{cases} -\left[S_{y0} + E_t \cdot \left(\dfrac{y}{\rho_i} - \varepsilon_y \right) \right] & y_y < y \le c \\ -\left(\dfrac{y}{y_y} \right) \cdot S_{y0} & -y_y \le y \le y_y \\ \left[S_{y0} + E_t \cdot \left(\dfrac{-y}{\rho_i} - \varepsilon_y \right) \right] & -c \le y < -y_y \end{cases} \tag{09}$$

$$\sigma_{sb}(y) = \frac{M(\rho_i) \cdot y}{I}, \quad -c \le y \le c \qquad \text{where } I = 2 \cdot \int_{-c}^{c} y^2 \cdot \left(\sqrt{radius_3^2 - y^2} - \frac{b_1}{2} \right) \cdot dy + \frac{b_1 \cdot h^3}{12} \tag{10}$$

$$\sigma^*_{res\_c}(y) = \sigma_{curv}(y) + \sigma_{sb}(y), \qquad -c \le y \le c \tag{11}$$

where, $\sigma_{curv}(y)$, $\sigma_{sb}(y)$ and $\sigma^*_{res\_c}(y)$ are, respectively, loading stress distribution, the spring-back stress distribution, and the residual stress distribution, all within phase 1. *I* is the area moment of inertia for a straight specimen.

Fig. 2.a shows, the $\sigma(\varepsilon)/S_{y0}$ vs ε evolution diagram of specimen points *a* and *b* during phase 1, and Fig. 2.b shows the specimen cross-section parameterized stress distribution in phase 1 – loading ($\sigma_{curv}(y)/S_{y0}$), spring back ($\sigma_{sb}(y)/S_{y0}$), and residual ($\sigma^{*}_{res\_c}(y)/S_{y0}$).

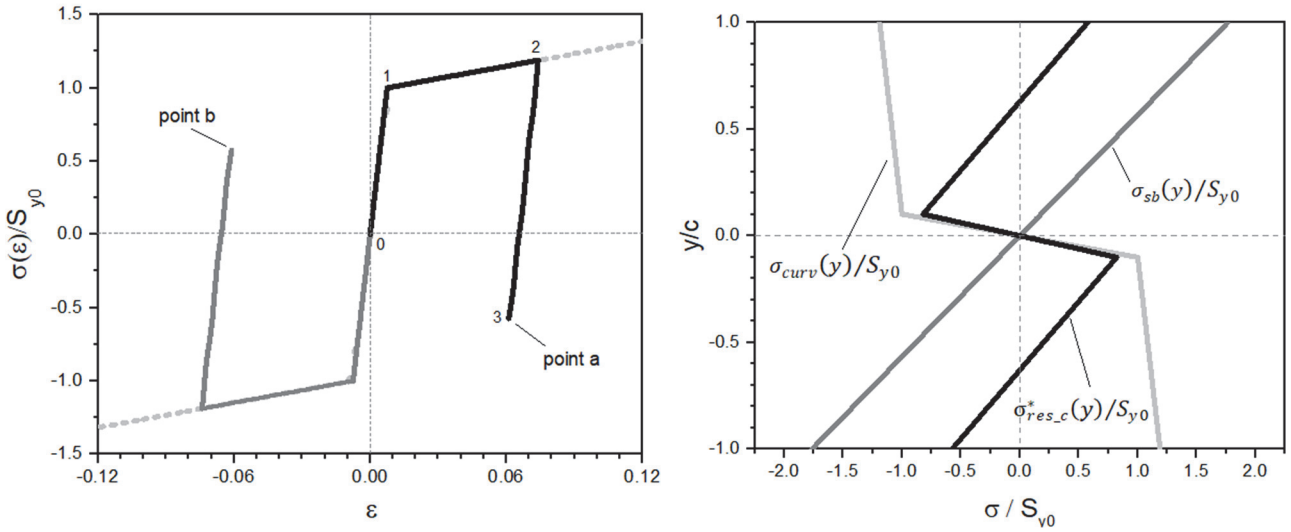

(a) (b)

Figure 2: (a) Specimen phase 1 graph ($\sigma(\varepsilon)/S_{y0}$ vs ε) for points *a* and *b*, and (b) Specimen cross-section parameterized stress distribution in phase 1 – loading ($\sigma_{curv}(y)/S_{y0}$), spring back ($\sigma_{sb}(y)/S_{y0}$), and residual ($\sigma^{*}_{res\_c}(y)/S_{y0}$).

Note that Fig.2.b axes are dimensionless to improve conceptual understanding. For instance, when $\sigma_{curv}(y)/S_{y0} = 1$, the material begins to yield. Also, an interesting point for mechanical parts severely yielded is that the residual stresses at the elastic-plastic border ($y/c = \pm y_y/c$) are bigger than the residual stresses at the external surfaces ($y/c = \pm 1$).

Combining the residual stress and the fatigue approaches

At the end of phase 1, the specimen cross-section stress distribution $\sigma^{*}_{res\_c}(y)$ is shown in Fig. 2.b. Before beginning phase 2 the specimen is turned upside down, obeying Eqn. (12) to convert $\sigma^{*}_{res\_c}(y)$ of Fig. 2.b into $\sigma_{res\_c}(y)$ of Fig. 3.

$$\sigma_{res\_c}(y) = -\sigma^{*}_{res\_c}(y), \qquad -c \le y \le c \tag{12}$$

Combining the residual stress and the fatigue stress loading distributions, using Eqns. (12) and Eqns. (4A.a) and (5A.a), results in Eqns. (13) and (14), as shown, graphically, in Fig. 3.

$$\sigma_{f\_max}(y) = \sigma_{res\_c}(y) + \sigma_{fad\_max}(y), \qquad -c \le y \le c \tag{13}$$

$$\sigma_{f\_min}(y) = \sigma_{res\_c}(y) + \sigma_{fad\_min}(y), \qquad -c \le y \le c \tag{14}$$

Fig. 3 shows the specimen cross-section stress distribution resulting from Eqns. (4A.a, 5A.a, 12, 13, 14). Both, $\sigma_{fad\_max}(y)/S_{y0}$ and $\sigma_{fad\_min}(y)/S_{y0}$ of Fig. 3.a and 3.b, respectively, have elastic stress distribution, but for the $\sigma_{f\_max}(y)/S_{y0}$ distribution, shown in Fig.3.a, it seems to have some yielding at external specimen surfaces. The main reason for applying such severe combined loading is to impose short lives on the specimens, intending to finish the experimental part of this research in a reasonable period.

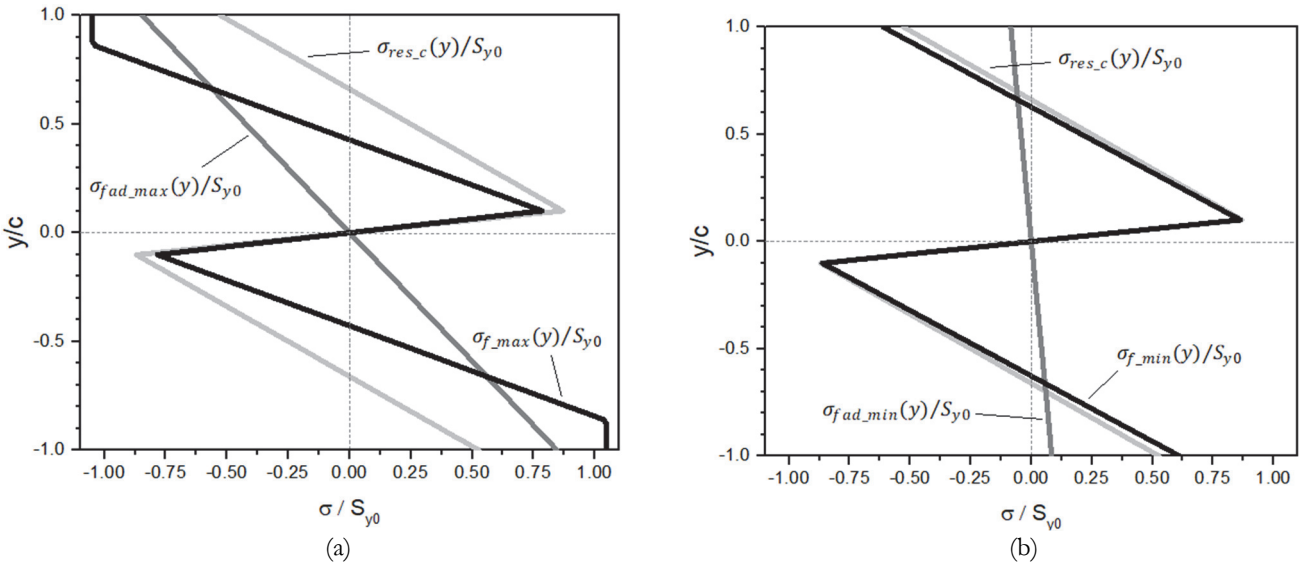

Figure 3: Phase 2 - Specimen cross-section loading stress distribution: (a) maximum and (b) minimum.

EXPERIMENTAL SETUP

The experimental part of this research was done in LAMAT Laboratory (https://dippg.cefet-rj.br/ppemm/index.php/pt/laboratorios/57-estrutura/296-laboratorio-de-materiais-lamat) of the Federal Center for Technological Education Celso Suckow da Fonseca - CEFET/RJ (https://www.cefet-rj.br/), in Rio de Janeiro, Brazil. It was used a servo-hydraulic material testing machine INSTRON 8801 of 100 kN of capacity, with a three-point bending grip setup with a phase 2 specimen positioned, as shown in Fig.4.a. The frequency of the fatigue test was limited to 10 Hz, due to the difficulties in adjusting the PID feedback control for such flexible specimens. The fatigue test was made in load control, and an excessive displacement interlock was set to stop the test immediately after the specimen had failed. Fig. 4.b shows an example of the experimental graph output displacement vs load of a specimen in phase 2. Fig. 4.c shows the two specimens' groups (***a*** and ***b***) after phase 1, where the curvatures were imposed, before being used in phase 2 of the fatigue test.

Each specimen has 25 cm length, and cross-section nominal values of 14 mm x 6 mm, which were taken from the manufacturer's wire spools of cold-drawn steel wires. Figs. 4.d and 4.e show examples of specimens' final fractures, from an external and an internal point of view.

In Fig. 4.b the abscissa axis shows the displacement of the piston rod, and the ordinate axis shows the load cell measurements during the fatigue test. The test began with the cycles positioned at the right part of the graphic. As the test heads towards the end, the distance between cycles increases until the specimen final failure, when the excessive displacement activates the interlock, ending the test. In the macrography of Fig. 4.e, it is possible to see a fatigue crack propagation region (the smooth region at the cross-section superior area) and a final failure region (the rough surface at the cross-section central area).

RESULTS AND DISCUSSION

In the experimental part of this research, an unexpected behavior of the tested specimens occurred. The specimens submitted to phases 1 and 2 had surprisingly long lives. The experimental results are summarized from the experimental approach of the original research developed in Zaidan [17], which is not entirely available because of a confidentiality agreement. Nevertheless, the results presented in the text are sufficient to support the development of the proposed analytical model.

It was initially assumed that the specimens taken from the manufacturer's wire spools of cold-drawn steel wires, did not have appreciable residual stress. As the specimens were taken from the manufacturer's wire spools, they were marked on the upper side with a yellow marker. The specimens were divided into groups ***a***, and ***b***. These groups were related to how the specimens were positioned on the 3-point bending gripper, with the wire's original yellow marking **a**bove or **b**elow. The objective was to verify if the specimen side, with the yellow marking top side or the bottom side, affects the specimen's

fatigue performance. Fig. 5 shows the theoretical SN curve (SN_{teo} 0%), with experimental results of groups ***a***, and ***b***, each group with three specimens, and the notable point *OF*.

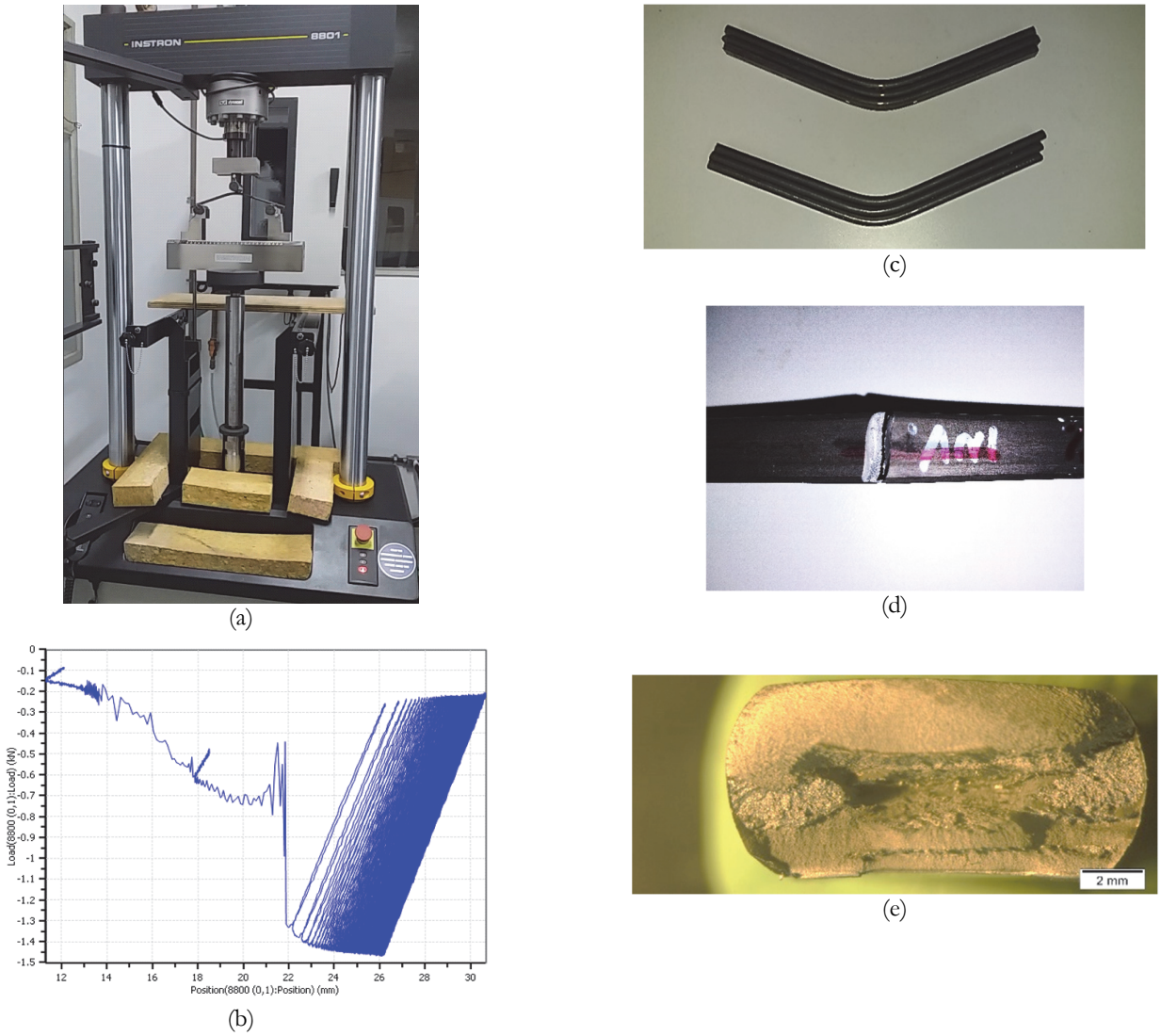

Figure 4: Experimental setup – (a) Servo-hydraulic material testing machine INSTRON of 100 kN of capacity, (b) Experimental graph output displacement vs load of a specimen in phase 2 (c) Groups ***a*** and ***b*** specimens after phase 1. Specimen failed after phase 2 – (d) external view and (e) internal view (macrography).

The fatigue results for both specimen groups ***a*** and ***b*** eventually show that they were quite similar. So, it was taken the average of the number of cycles generated by the specimens of both groups, N_{exp}, shown in Fig. 5. Note that the number of cycles that the specimens failed N_{exp} exceeded the number of cycles estimated by the proposed fatigue model N_{teo}. With the aid of Eqns. (7A.a) and (7A.b), the equivalent alternate stress σ_{a_eq} and the number of cycles until fatigue failure, Nteo are estimated, which correspond to point OF of Fig. 5. In effect, the point of coordinates (N_{exp}, σ_{a_eq} / S_{y0}) is not on the theoretical SN curve (SN_{teo} 0%), described by Eqn. (2A). An explanation for this behavior is proposed next.

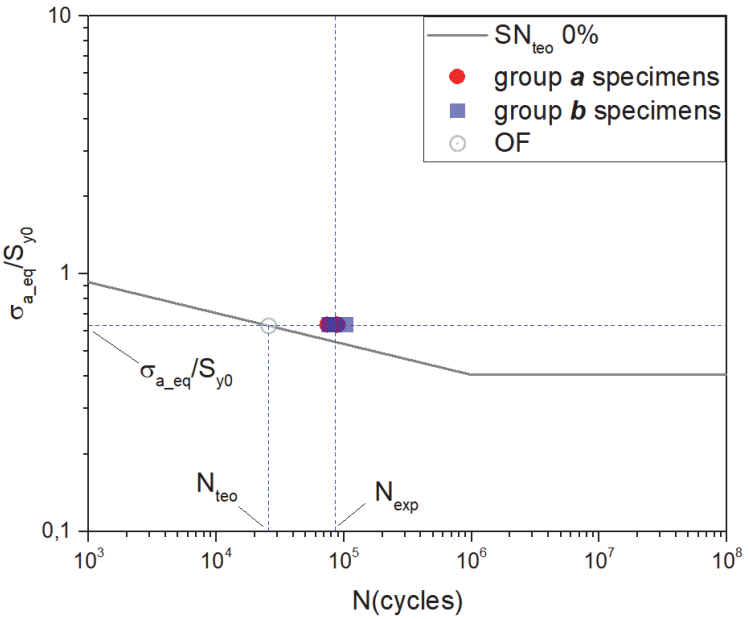

Figure 5: Theoretical SN curve (SN_{teo} 0%), with experimental results.

It was tentatively solved by adjusting the S_{ut0} for a higher value, considering |6%| residual strain present in specimen surfaces after phase 1, as shown in point *a* of Fig. 2.a. This S_{ut} correction generated a new theoretical SN curve (SN_{teo} 6%) of Eqn. (2A) approximating to the experimental results, but not sufficiently. Moving the SN curve more in the "right" direction, a new SN curve was proposed, named the hypothetical SN curve (SN_{hyp} 6%), which passes through the fatigue experimental points. To describe the SN_{hyp} 6%, shown in Fig. 6, Eqn. (15) is proposed

$$S_f^{hyp} = \begin{cases} S_{ut} \cdot (N)^{\left(\frac{1}{3}\cdot\log(f)\right)}, & 10^0 \le N \le 10^3 \\ a_{hyp} \cdot (N)^{b_{hyp}}, & 10^3 < N < 10^6 \\ a_{hyp} \cdot (10^6)^{b_{hyp}}, & N \ge 10^6 \end{cases} \qquad a_{hyp} = \frac{\sigma_{a\_eq\_6}}{(N_{exp})^{b_{hyp}}} \qquad b_{hyp} = b_{teo} \tag{15}$$

where S_f^{hyp} is the hypothetical fatigue resistance, and a_{hyp} and b_{hyp} are hypothetical constants. Note that equivalent alternate stress $\sigma_{a\_eq\_6}$ of Eqn. (15.b) uses the same Eqn. (7A.a), but with two differences: a) the material has a 6% residual strain, instead of 0%, and b) the loading combines residual and fatigue stresses, instead of only fatigue stresses.

Considering that the average experimental number of cycles N_{exp} is the only undeniable experimental result, two different approaches were proposed to explain the difference between N_{teo} and N_{exp}. The two notable points related to the two different proposed approaches are shown in Fig. 6.

The first approach requires the existence of the new SN curve, called SN_{hyp} 6%, which is described by Eqn. (15). This approach receives the name of "resistance increase". One explanation for this proposition can be reached through the modification of the miscellaneous-effects factor k_f of Eqn. (1A), substituting the value 1 by a value greater than one, rising the S_e value, and therefore generating the a_{hyp} and b_{hyp} values of SN_{hyp} 6% curve. The point $(N_{exp}, \sigma_{a\_eq}^{RI} / S_{y0})$ is represented by a black triangle RI on the SN_{hyp} 6% curve in Fig. 6:

$$\sigma_{a\_eq}^{RI} = a_{hyp} \cdot (N_{exp})^{b_{hyp}} \tag{16}$$

The second approach maintains the original SN curve, called SN_{teo} 0%, but reduces σ_{a_eq} originally estimated by Eqn. (7A.a) to $\sigma_{a\_eq}^{SR}$ of Eqn. (17). This approach receives the name "stress reduction". This effect can appear, for instance, by the existence of superficial residual compressive stress in function of the manufacturing process, such as cold rolling. This approach doesn't modify the fatigue limit as the former approach but actuates only diminishing the effective tensile stresses that is acting in the specimen's cross-section area. See Gothivarekar et al. [18] for a schematic cross-section residual stress distribution representation after a cold rolling process. The point $(N_{exp}, \sigma_{a\_eq}^{SR} / S_{y0})$ is represented by a black inverted triangle SR on the SN_{teo} 0% curve in Fig. 6:

$$\sigma_{a\_eq}^{SR} = a_{teo} \cdot \left(N_{exp} \right)^{b_{teo}} \tag{17}$$

From the mechanical engineering point of view, this second approach, named "stress reduction", is more reasonable. Fig. 6 resumes, in a graphical form, the proposed SN curves and the notable points.

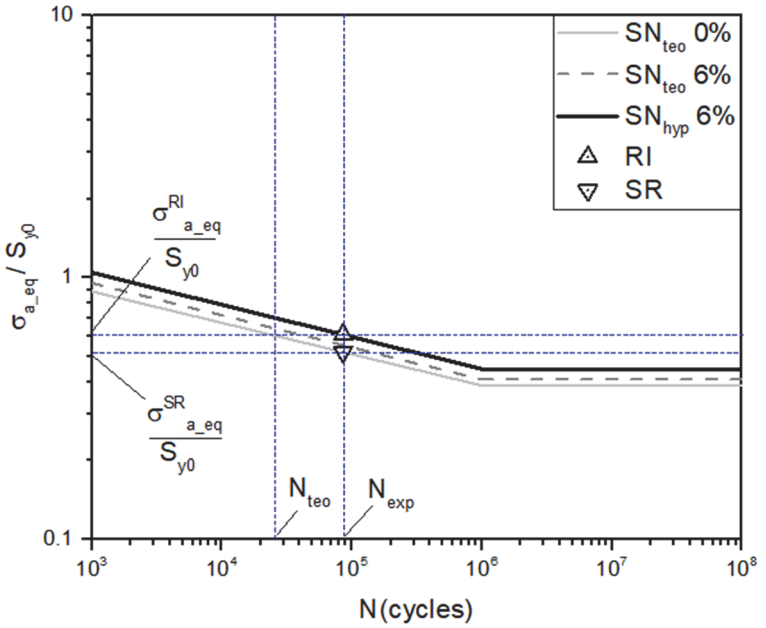

Figure 6: Proposed SN curves and the notable points.

The RI and SR stresses are calculated, respectively, through Eqns. (16) and (17), positioned in different SN curves, respectively, on SN_{hyp} 6% and on SN_{teo} 0%, but have the same number of cycles, N_{exp}. Comparing OF point (only fatigue) of Fig 5, with the SR or RI points (both for fatigue plus residual stress) of Fig. 6, there is a perceptible difference in cycles to failure between N_{teo} and N_{exp}, of almost an order of magnitude. The compressive superficial residual stress generated by the wire lamination could extend the specimen's life, even though the specimen has been submitted, in phase 1, to severe tensile residual stress. In summary, it is proposed that the lowering $\sigma_{a\_eq}^{RI}$ to a new equivalent alternate stress $\sigma_{a\_eq}^{SR}$ is feasible by the existence of superficial compressive residual stress caused by the lamination process, which can be estimated as:

$$\sigma_{a\_eq}^{lam} = \sigma_{a\_eq}^{SR} - \sigma_{a\_eq}^{RI} \tag{18}$$

Besides the superficial compressive residual stress caused by the lamination process, estimated by Eqn. (18), it is possible to propose an estimation of the effect on the cross-section residual stress distribution resulting from the specimen cold rolling process:

$$\sigma_{res_1}(y)=\begin{cases}\sigma_{a\_eq}^{lam} & y_1 \le y \le c \\ -\left(\dfrac{c-y_1}{y_1}\right)\cdot\sigma_{a_{eq}}^{lam} & y_1 \le y \le -y_1 \\ \sigma_{a\_eq}^{lam} & -y_1 \le y \le -c\end{cases} \quad \text{where, } y_1 = 0.8\cdot c \tag{19}$$

The cross-section semi-height, for tensile stress is yl and for compressive stress is (c - yl). Its value was chosen arbitrarily since this information is relatively scarce in technical literature, usually presented only qualitatively, as in Gothivarekar et al. [18].

Adding Eqn. (19) to Eqns. (13) and (14), generates the maximum and minimum specimen's cross-section stress distribution, respectively, Eqns. (20) and (21):

$$\sigma_{f\_max}^{*}(y)=\sigma_{f\_max}(y)+\sigma_{res_1}(y) \qquad -c \le y \le c \tag{20}$$

$$\sigma_{f\_min}^{*}(y)=\sigma_{f\_min}(y)+\sigma_{res_1}(y) \qquad -c \le y \le c \tag{21}$$

Finally, adding all the residual stress (from the curvature in phase 1 and from the cold rolling process):

$$\sigma_{res}(y)=\sigma_{res\_c}(y)+\sigma_{res_1}(y) \qquad -c \le y \le c \tag{22}$$

Fig. 7.a and 7.b exhibit the graphical representation, respectively, for Eqns. (20) and (21), and for Eqn. (22).

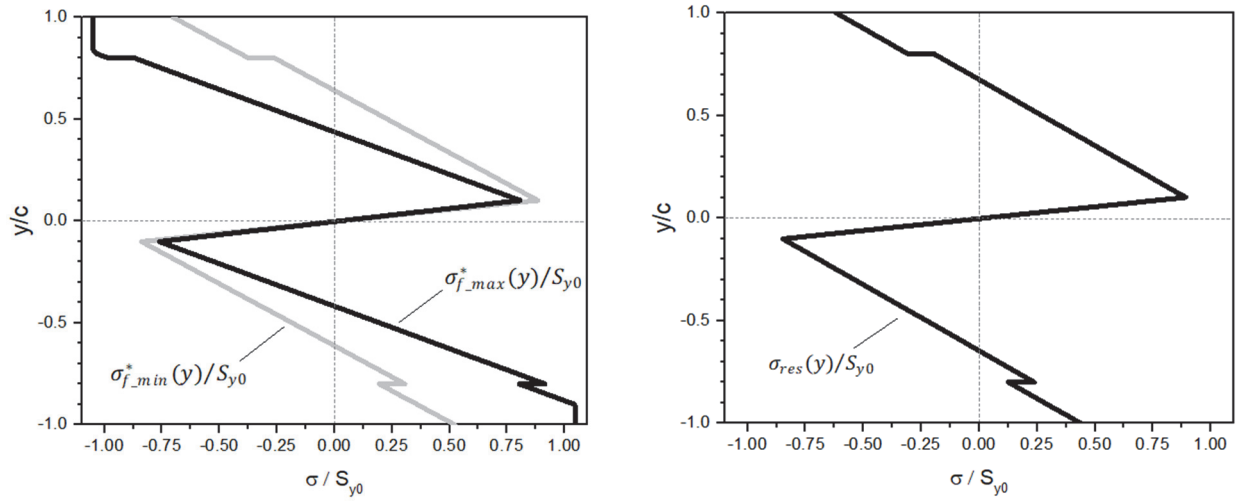

Figure 7: Specimen cross-section stress distribution: (a) in Phase 2 and (b) after Phase 2.

Fig. 7.a shows the effect of the lamination in the specimen's cross-section loading stress distribution during phase 2. Fig. 7.b shows the sum of all residual stresses, that exist after phase 2. Comparing Fig. 7.a with Fig. 3.a, there is a reduction of superficial tensile stress at extrados (y = - c) and increasing the compressive stress at intrados (y = + c). Also, note in Fig. 7.b, that the residual stresses at the elastic-plastic border ($y/c = \pm y_y/c$) are bigger than at the external surfaces ($y/c = \pm 1$).

CONCLUSIONS

An analytical model was built in detail, combining fatigue and residual stresses, to check the effect of residual stress on the fatigue performance of partially yielded cold-drawn steel wire specimens. All equations and their graphical representations were explicitly presented. Initially, it was assumed that the specimens, taken from the manufacturer's wire spools, did not have appreciable residual stress. So, a curvature was imposed on specimens to generate

a specified distribution of residual stresses. In sequence, the specimens were subjected to time-variable experimental bending loading until fatigue failure occurred. It was realized that the number of cycles the specimens spent up to failure was nearly one order of magnitude larger than those theoretically predicted. It was recognized that the residual stresses imposed by curvature on specimens were insufficient to remove the former beneficial compressive residual stresses, probably generated by cold rolling manufacturing. Two approaches were designated, with success, to adjust the analytical model to encompass the number of cycles difference. An analytical estimation of the level of the former superficial compressive residual stresses was also achieved. These results can contribute to improving the knowledge about the effectiveness of residual stress in the fatigue performance of partially yielded cold-drawn steel wires, including the initially unexpected beneficial effects promoted by the cold rolling fabrication process.

REFERENCES

[1] Laterza, M., D'amato, M. and Casamassima, V.M. (2017). Stress-Life Curves Method for Fatigue Assessment of Ancient Brick Arch Bridges. International Journal of Arch. Heritage. 11(6), pp. 843-858. DOI: https://doi.org/10.1080/15583058.2017.1315621.

[2] Teoh, S.H. (2000). Fatigue of biomaterials: a review. International Journal of Fatigue, 22, pp. 825–837.

[3] Tabatabaeian, A., Ghasemi, A.R., Shokrieh, M.M., Marzbanrad, B., Baraheni, M., Fotouhi, M. (2022). Advanced Engineering Materials; 24(3), pp. 2100786. DOI: https://doi.org/10.1002/adem.202100786.

[4] Crandall, S.H., Dahl, N.C. and Lardner, T.J. (1978). An Introduction to the Mechanics of Solids. Second Edition with SI units, McGraw Hill International Editions.

[5] Stok, B. and Halilovic M. (2008). Analytical solutions in elastoplastic bending of beams with rectangular cross-section. Applied Mathematical Modelling; 33, pp. 1749-1760. DOI: https://doi.org/10.1016/j.apm.2008.03.011.

[6] Rimovskis, S. and Sabaliauskas, A. (2012). Analysis of Rectangular and Circular Cross-section Power Hardening Elements under Pure Bending. International Journal of Materials Engineering, 2(6), pp.84-89. DOI: https://doi.org/10.5923/j.ijme.20120206.03.

[7] Castro, J.T.P. and Meggiolaro, M.A. (2016). Fatigue Design Techniques, Volume 2: Low-Cycle and Multiaxial Fatigue, 1. ed., Scotts Valley, CA 95066, USA: CreateSpace.

[8] Jirásek, M. and Bazant, Z.P. (2002). Inelastic Analysis of Structures. John Wiley and Sons Ltd.

[9] De Castro, F.A., Kenedi, P.P., Vignolli, L.L. and Riagusoff, I.I.T. (2021) Residual stress distribution in built-in beams. Proceedings of the Institution of Mechanical Engineers Part L-Journal of Materials-Design and Applications. 235(1), pp. 216-231. DOI: https://doi.org/10.1177/1464420720958617.

[10] Schajer, G.S. (2013). Practical Residual Stress Measurement Methods. Wiley.

[11] Atienza, I., and Elices, M. (2003). Influence of residual stresses in the tensile test of cold-drawn wires. Materials and Structures, 36, pp. 548-552.

[12] McClung, R. C. (2007). A literature survey on the stability and significance of residual stresses during fatigue. Fatigue & Fracture of Engineering Materials and Structures, 30(3), pp.173-205. DOI: https://doi.org/10.1111/j.1460-2695.2007.01102.x.

[13] Webster, G.A. and Ezielo, A.N. (2001). Residual stress distributions and their influence on fatigue lifetimes. International Journal of Fatigue. 23 (1), pp. 375-383. DOI: https://doi.org/10.1016/S0142-1123(01)00133-5.

[14] James, M.N., Hughes, D.J., Chen, Z., Lombard, H., Hattingh, D.G., Asquith, D., Yates, J.R., Webster, P.J. (2007) Residual stresses and fatigue performance. Engineering Failure Analysis. 14(2), pp. 384-395. DOI: https://doi.org/10.1016/j.engfailanal.2006.02.011.

[15] Vaara, J., Kunnari, A. and Frondelius, T. (2020). Engineering Failure Analysis. 110, pp.104379. DOI: https://doi.org/10.1016/j.engfailanal.2020.104379.

[16] Zaidan, L.D., Buarque, Y. C., Kenedi, P.P., de Souza, L. F. G. (2022). Fatigue and residual stresses - a deleterious combination. In: Proceedings of the International Symposium on Solid Mechanics, MECSOL 2022, Campinas - SP, Brazil.

[17] Zaidan, L.D. (2023). Influência da Tensão Residual na vida à Fadiga de Estruturas Parcialmente Plastificadas, Master Thesis (in Portuguese), Centro Federal de Educação Tecnológica Celso Suckow da Fonseca - CEFET/RJ, Brazil.

[18] Gothivarekar, S., Coppieters, S., Van de Velde, A., Debruyne, D. (2020). Advanced FE model validation of cold-forming process using DIC: Air bending of high-strength steel. Int J Mater Form; 13, pp. 409-421. DOI: https://doi.org/10.1007/s12289-020-01536.

[19] Budynas, R.G. and Nisbett, J.K. (2015). Shigley's Mechanical Engineering Design. McGraw-Hill, 10th Edition.

APPENDIX

Fatigue basics

The fatigue part of the analytical model is explicitly presented and commented on, based on the classical approach, as in Budynas et al. [19]. The fatigue limit S_e is estimated as:

$$S_e = k_a \cdot k_b \cdot k_c \cdot k_d \cdot k_e \cdot k_f \cdot 0.5 \cdot S_{ut} = \left(4.51 \cdot \left(S_{ut}\right)^{-0.265}\right) \cdot \left[\frac{0.808 \cdot \sqrt{b_2 \cdot h}}{7.62}\right]^{-0.107} \cdot 1 \cdot 1 \cdot 1 \cdot 1 \cdot 0.5 \cdot S_{ut} \quad (1A)$$

where, k_a, k_b, k_c, k_d, k_e, and k_f are the modifying factors. b_2 and h are used in mm and S_{ut} are used in MPa. The theoretical SN curves SN_{teo} 0% and SN_{teo} 6%, shown in Fig. 6, is generated by Eqn. (2A):

$$S_f = \begin{cases} S_{ut} \cdot N^{\left(\frac{1}{3} \cdot \log(f)\right)} & 10^0 \le N < 10^3 \\ a_{teo} \cdot N^{b_{teo}} & 10^3 \le N \le 10^6 \\ S_e & N > 10^6 \end{cases} \qquad a_{teo} = \frac{\left(f \cdot S_{ut}\right)^2}{S_e} \quad b_{teo} = -\frac{1}{3} \cdot log\left(\frac{f \cdot S_{ut}}{S_e}\right) \quad (2A)$$

S_f is the theoretical fatigue resistance, f is the fatigue strength fraction, N is the number of fatigue cycles, a_{teo} and b_{teo} are theoretical constants. Note that in Eqns. (1A) and (2A), for the as-received straight specimen, with no residual stress, the S_e, S_f, and S_{ut} are substituted by S_{e0}, S_{f0}, and S_{ut0}, respectively. This material is generically labeled as 0%. For the curved specimen at the beginning of phase 2, a 6% superficial residual strain is built, as shown in Fig. 2.a. Then, S_e, S_f, and S_{ut} are substituted by S_{e6}, S_{f6}, and S_{ut6}. This material is generically labeled as 6%. The fatigue stress distributions σ_{fad_max} (y) and σ_{fad_min} (y), at the middle of the specimen, can be estimated by:

$$M_{min} = P_{min} \cdot \frac{L}{4} \qquad M_{max} = P_{max} \cdot \frac{L}{4} \quad (3A)$$

$$\sigma_{fad\_max}(y) = \frac{M_{max} \cdot y}{b_2 \cdot h \cdot exc \cdot \left(radius_2 - c\right)} \qquad \sigma_{x\_max} = \sigma_{fad\_max}(-c) \quad (4A)$$

$$\sigma_{fad\_min}(y) = R \cdot \sigma_{fad\_max}(y) \qquad \sigma_{x\_min} = \sigma_{fad\_min}(-c) \quad (5A)$$

$$exc = \rho_i - radius \qquad radius = h \Big/ \left[ln\left(\frac{\rho_i + \frac{h}{2}}{\rho_i - \frac{h}{2}}\right)\right] \quad (6A)$$

$$\sigma_{x_m} = \frac{\sigma_{x\_min} + \sigma_{x\_max}}{2} \qquad \sigma_{x_a} = \frac{\sigma_{x\_max} - \sigma_{x\_min}}{2}$$

where *exc* and *radius* are well-known variables of curved beams theory (because the specimens in phase 2 are curved). P_{min} and P_{max} are the minimum and maximum fatigue transversal loads, respectively. Consequently, M_{min} and M_{max} are, respectively, the minimum, and the maximum fatigue bending moments in the middle of the specimen. σ_{x_min} , σ_{x_max}, σ_{x_m} and σ_{x_a} are respectively, the minimum, the maximum, the average, and the alternate fatigue bending stress at y = - c (point *b* of Fig.1.d), in the middle of the specimen. *R* is the stress ratio.

Note that the shear stresses are null, $\tau_{xy_m} = \tau_{xy_a} = 0$, as the torsion stress is null, and the shear stresses caused by the transversal load are disregarded. So, using the von Mises criterion, it is possible to show that the Mises average stress is

$\sigma_m = \sigma_{x\_m}$ and the Mises alternate stress $\sigma_a = \sigma_{x\_a}$. Eqn. (7A.a) converts the stresses σ_m and σ_a to one unique equivalent alternate stress σ_{a_eq}, based on Goodman Criterion, which is a Fatigue failure criterion which includes, in addition to the alternate stress, the average ones. The estimation of the theoretical finite life of the specimens N_{teo} is done:

$$\sigma_{a\_eq} = \left(\frac{1}{1 - \left(\frac{\sigma_m}{S_{ut}} \right)} \right) \sigma_a \qquad N_{teo} = \left(\frac{\sigma_{a\_eq}}{a_{teo}} \right)^{1/b_{teo}} \quad \text{for } 10^3 \le N \le 10^6 \tag{7A}$$

When Eqn. (7A) uses the mechanical properties of an as-received material (labeled as 0%), with no residual stress, S_e, S_f, and S_{ut} are substituted by S_{e0}, S_{f0}, and S_{ut0}, respectively. The point $(N_{teo}, \sigma_{a\_eq} / S_{y0})$ is on the SN_{teo} 0% curve, which is graphically shown on Fig.5.